Local atomic structure around Ni, Nb, and Zr atoms in Ni-Nb-Zr-H glassy alloys studied by x-ray absorption fine structure method

doi: 10.1063/1.3143039

Local atomic structure around Ni, Nb, and Zr atoms in Ni–Nb–Zr–H glassy alloys studied by x-ray absorption fine structure method

H. Oji,[1,2,a] K. Handa,[3] J. Ide,[3] T. Honma,[1] S. Yamaura,[4] A. Inoue,[4] N. Umesaki,[1] S. Emura,[5] and M. Fukuhara[4]

[1]*Industrial Application Division, Japan Synchrotron Radiation Research Institute, 1-1-1 Kouto, Sayo-cho, Sayo-gun, Hyogo 678-5198, Japan*
[2]*SPring-8 Service Co., Ltd., 2-23-1 Kouto, Kamigori-cho, Ako-gun, Hyogo 678-1205, Japan*
[3]*Institute for Chemical Research, Kyoto University, Gokasho, Uji, Kyoto 611-0011, Japan*
[4]*Institute for Materials Research, Tohoku University, 2-1-1 Katahira, Aoba, Sendai 980-8577, Japan*
[5]*Institute of Scientific and Industrial Research, Osaka University, 8-1 Mihoga-oka, Ibaraki, Osaka 567-0047, Japan*

(Received 12 February 2009; accepted 4 May 2009; published online 10 June 2009)

To elucidate hydrogen effects on the atomic configuration of Ni–Nb–Zr–H glassy alloys exhibiting proton-tunneling-induced Coulomb oscillation, we investigated the local atomic configuration around the Ni, Nb, and Zr atoms by x-ray absorption fine structure (XAFS) method. The analysis of the XAFS spectra indicates that there is the significant difference in structural response between the Zr 30 and the Zr 40 at. % alloys when hydrogen atoms are charged; charging the hydrogen atoms basically does not alter the local structures around the three atoms for the Zr 30 at. % alloy but induces the elongation of the Zr–Zr, Zr–Nb, and Nb–Ni distances for the Zr 40 at. % alloy. The distorted icosahedral $Zr_5Ni_5Nb_3$ clusters assembled in randomly packed manners for the possible models in the Ni–Nb–Zr glassy alloy are proposed. The sites where hydrogen atoms occupy are also inferred. © *2009 American Institute of Physics*. [DOI: 10.1063/1.3143039]

I. INTRODUCTION

Since Ben-Jacob and Gefen[1] first proposed a quantum oscillation in small current-driven junctions, the Coulomb blockade effect by quantum-dot tunneling has been the current topic in physics.[2–5] Recently, Fukuhara *et al.*[6] observed the electric current-induced voltage oscillation in $(Ni_{42}Nb_{28}Zr_{30})_{1-y}H_y(0.052 \leq y \leq 0.152)$, $[(Ni_{0.6}Nb_{0.4})_{100-x}Zr_x]_{1-y}D_y$ ($x=30$, 35, 40, and 45, $0.091 \leq y \leq 0.148$),[7] and Ti–Ni–Cu–H (Ref. 8) glassy alloys. Furthermore, the frequency of the $(Ni_{36}Nb_{24}Zr_{40})_{0.901}H_{0.099}$ glassy alloy decreased remarkably with the increasing capacitance (C) and resistance (R) in the dc/ac circuit at room temperature.[9] This resembles the discharging behavior in which a constant voltage-discharge tube with a parallel condenser and a high resistance causes block oscillations, which are derived from the charging and discharging of the capacitance. This phenomenon was considered as the Coulomb oscillation observed in quantum dots, where it results from the tunneling of proton (deuteron) at mesoscopic tunnel junction. In this case, we can image zigzag paths linking the atomic Zr–H–□–H–Zr array (□: vacancy barrier) corresponding to a single Coulomb-blockade tunneling junction between the tetrahedrons belonging to each icosahedral cluster. If this speculation is true, it is surprising that the tunneling junctions are natively formed in the Ni–Nb–Zr alloy, which is a typical metal-metal-type alloy with familiar transition elements. Thus it is very important to analyze the atomic configuration of the Ni–Nb–Zr–H alloys consisting of atomic clusters in order to verify the possibility of the proton tunneling.

According to the results of neutron diffraction by Westlake *et al.*,[10] deuterium atoms preferentially occupy the sites coordinated tetrahedrally by four zirconium atoms (hereafter referred to as tetrahedral Zr site) in the ZrNiD glassy alloy. The results of total neutron scattering and inelastic neutron scattering by Suzuki *et al.*[11] also indicate that hydrogen atoms initially prefer to occupy the tetrahedral Zr site in the hydrogenated ZrNi glassy alloy up to about 25 at. % hydrogen content. Hence, by analogy, Fukuhara *et al.* inferred that hydrogen (deuteron) atoms preferentially occupy the tetrahedral Zr site in the Ni–Nb–Zr alloys and tunnel from an occupied site to the other unoccupied site when electric field is applied. Although there are a few reports on the structure of ternary metal/metal-type bonding glassy alloys without hydrogen[12–14] and those with hydrogen,[15,16] the structure of the Ni–Nb–Zr glassy alloys including hydrogen has not been clarified enough to confirm their hypothesis.

To elucidate the hydrogen effect on the metallic bonding configuration in this study, we measured the x-ray absorption fine structure (XAFS) spectra of the Ni–Nb–Zr glassy alloy films with two different chemical compositions, i.e., $Ni_{42}Nb_{28}Zr_{30}$ (hereafter referred to as Zr30–H0) and $Ni_{36}Nb_{24}Zr_{40}$ (Zr40–H0), and their hydrogen-charged ones, i.e., $(Ni_{42}Nb_{28}Zr_{30})_{0.91}H_{0.09}$ (Zr30–H9) and $(Ni_{36}Nb_{24}Zr_{40})_{0.89}H_{0.11}$ (Zr40–H11). Although both Zr30–H0 and Zr40–H0 are amorphous,[17] the hydrogen permeation characteristic of the latter is higher than that of the former.[18] XAFS, as one category of x-ray absorption spectroscopy, is a powerful tool for the structural analysis of amorphous materials because the useful information on the local structure around an element of interest can be obtained by this method by tuning the photon energy to the absorption edge of the

[a]Electronic mail: oji-h@spring8.or.jp.

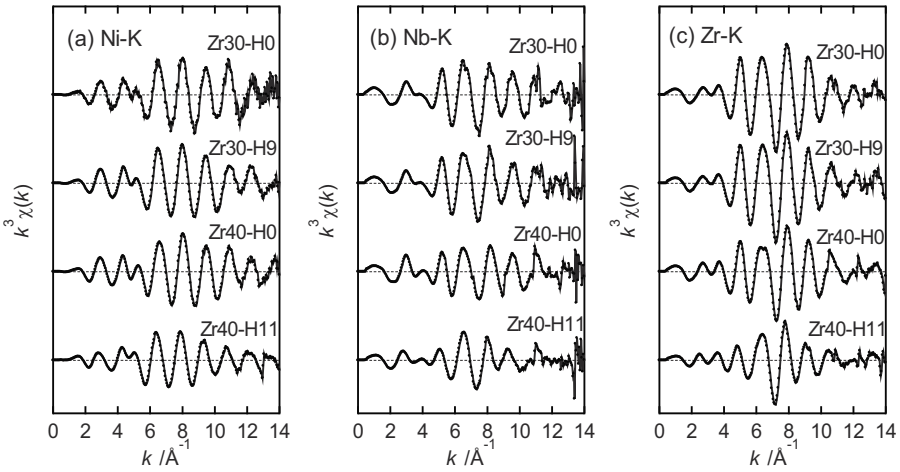

FIG. 1. XAFS oscillations extracted from the x-ray absorption spectra of Zr30–H0, Zr30–H9, Zr40–H0, and Zr40–H11 glassy alloys measured at (a) Ni, (b) Nb, and (c) Zr *K*-edges. Note that the oscillations shown here are weighted by k^3.

specific element.[19] By analyzing the XAFS oscillation in the x-ray absorption spectra of the Ni–Nb–Zr(−H) alloys measured at the Ni, Nb, and Zr *K*-edges, we obtained the information of the local structure around these three elements. The results revealed that there are significant differences in the behavior of the structural change between the Zr 30 and Zr 40 at. % samples when hydrogen is charged.

II. EXPERIMENTAL

Rotating wheel methods under an argon atmosphere were used for the preparation from argon arc-melted ingots of the amorphous Zr30–H0 and Zr40–H0 alloy ribbons. The width and thickness of the ribbons were ~2.5 mm and 16–26 μm, respectively. Hydrogen charging was carried out electrolytically in 0.5 M H_2SO_4 and 1.4 g/L thiourea (H_2NCSNH_2) at room temperature using current densities of 30 A/m^2.[6] The amounts of the hydrogen absorbed in the specimens were measured by the inert gas carrier melting-thermal conductivity method. We used hydrogen-doped samples of Zr30–H9 and Zr40–H11 in comparison with the Zr30–H0 and the Zr40–H0 alloys.

The XAFS spectra were measured at the bending-magnet beamline BL14B2 (Ref. 20) of the large-scale synchrotron radiation facility (SPring-8) in Hyogo, Japan. The incident x rays were monochromatized by a silicon double crystal monochromator. The net planes used are (311) for the Nb and Zr *K*-absorption edges and (111) for the Ni *K*-absorption edge. The higher harmonics of the incident x rays were reduced by two Rh-coated mirrors. The spectra were taken in a normal transmittance mode. To obtain the appropriate x-ray absorption intensity, the two sheets of ribbon had to be stacked in the Nb *K*- and Zr *K*-edge measurements, while one sheet of ribbon was in optimum thickness for the Ni *K*-edge measurements. The samples were cooled down to ~20 K in order to avoid thermal disturbance. The extraction of the XAFS oscillation from the spectra, normalization by edge-jump, and Fourier transformation were performed by a code Athena.[21] The curve-fitting analysis was carried out in *R*-space by a code Artemis.[21] The XAFS oscillation function $\chi(k)$ is written as

$$\chi(k) = \frac{S_0^2 N_i F_i(k)}{kr_i^2} \exp\left(-2k^2\sigma_i^2 - \frac{2r_i}{\lambda_i(k)}\right) \sin[2kr_i + \phi_i(k)], \tag{1}$$

where the electron wave vector k is defined as

$$k = [2m(E - E_0)/\hbar^2]^{1/2}, \tag{2}$$

S_0^2 is the amplitude reduction factor, N_i is the number of atoms in the ith shell, $F_i(k)$ is the backscattering amplitude of the ith neighbor atom, r_i is the mean distance between the absorbing atom and the ith shell, σ_i^2 is the mean squared relative disorder (MSRD) between the absorbing atom and an atom in the ith shell, $\phi_\iota(k)$ is the phase shift, and $\lambda_\iota(k)$ is the mean-free path of the photoelectron. In the code Artemis, $F_i(k)$, $\phi_\iota(k)$, and $\lambda_\iota(k)$ were theoretically calculated by a code FEFF6L, and then the other parameters N_i, r_i, σ_i^2, and E_0 are treated as fitting parameters in the curve-fitting analysis. In this analysis, S_0^2 is assumed to be unity.

III. RESULTS

A. XAFS oscillations and their Fourier transforms

Figs. 1(a)–1(c) show the k^3-weighted XAFS oscillations extracted from the absorption spectra of the Zr30–H0, Zr30–H9, Zr40–H0, and Zr40–H11 glassy alloys measured at the Ni, Nb, and Zr *K*-edges, respectively. All the oscillation patterns show simple curves, as typically seen for amorphous materials. The Zr *K*-edge XAFS oscillations of Zr30–H0 resemble to that of the Ni–Nb–Zr alloys with the same chemical composition reported by Sakurai *et al.*[15] The XAFS oscillations for all *K*-edges in Zr30–H0 is almost identical with those of Zr30–H9. However, the oscillations of Zr40–H11 are significantly different from those of Zr40–H0, indicating a distinct structural change caused by hydrogenation.

The absolute values of Fourier transforms (FTs) of the k^3-weighted XAFS oscillations ($|F(r)|$) are depicted in Figs. 2(a)–2(c) for the Ni, Nb, and Zr *K*-edge oscillations, respectively. The analyzed FT ranges are 2.7–13.3, 3.0–12.0, and 2.9–13.5 Å^{-1} for the Ni, Nb, and Zr *K*-edges, respectively. Each FT spectrum gives basically the information similar to the partial radial distribution function around the core-excited atoms. Note, however, that the apparent interatomic

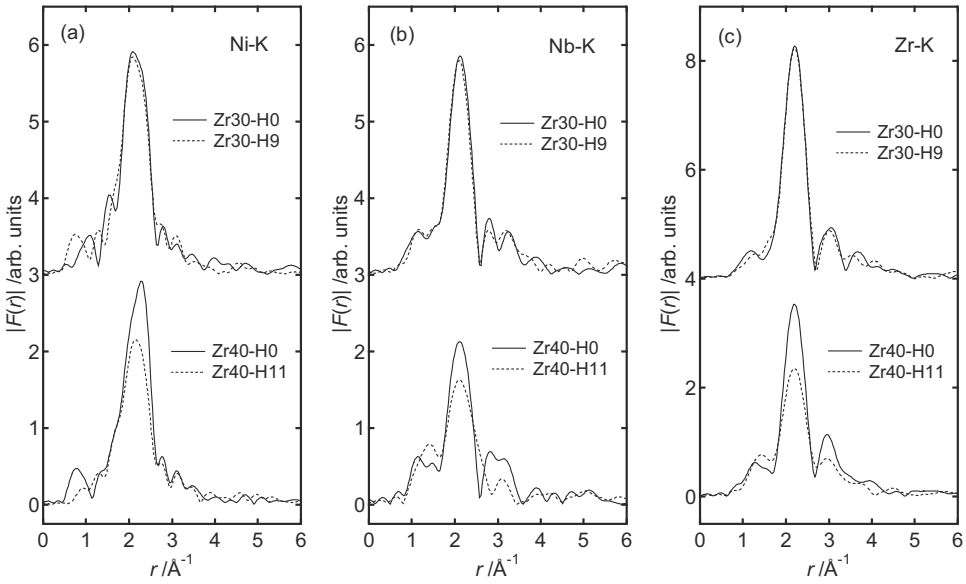

FIG. 2. The absolute values of FTs of k^3-weighted XAFS oscillations ($|F(r)|$) of Zr30–H0 (upper solid lines), Zr30–H11 (upper dotted lines), Zr40–H0 (lower solid lines), and Zr40–H11 (lower dotted lines) at (a) Ni, (b) Nb, and (c) Zr *K*-edges. The FT ranges analyzed are 2.7–13.3, 3.0–12.0, and 2.9–13.5 $Å^{-1}$ for Ni, Nb, and Zr *K*-edges, respectively.

distances in the spectra shift on the shorter side by several tenths of angstroms from the average values of the atomic distances obtainable in a diffraction method, since the phase shift correction has not been carried out.

At $r>4$ Å, there is no clear structure in the FT spectra for all the samples at the three absorption edges, indicating that there is mostly no longer-range ordering in the glassy alloys. The electron scattering from the atoms locating at longer position than 4 Å in these glassy alloys only piles up the background in FT spectra by a small amount.

The first nearest neighbor peaks of the FT spectra of the Ni *K*-edge for all the samples are asymmetrical in the shape [Fig. 2(a), suggesting that each of these peaks consists of two or more components. First, there should be two components which come from the Ni–Zr and Ni–Nb coordinations because the feature of the Ni coordination can be evaluated from the first nearest neighbor peaks at both the Nb and Zr *K*-edges, as discussed below. Second, the contribution of Ni–Ni to the peak cannot be ignored, taking the realistic structures of Ni–Zr and Ni–Nb bimetallic crystal alloys into consideration.[22–27] Thus, the first nearest neighbor peaks of the FT spectra on the Ni *K*-edge probably consist of at least three components (Ni–Zr, Ni–Nb, and Ni–Ni).

The first nearest neighbor peak at $r\sim2$ Å of the FT spectra for the Nb *K*-edge is symmetrical in shape, indicating that it consists of a single component [Fig. 2(b)]. Judging from the reported atomic structures of NiNb crystal alloys,[22,23] it is reasonable to assign this peak to the Nb–Ni coordination. The origin of the complex feature around 2.6–3.6 Å is not clear at present time. It may be due to overlapping of several components which come from the Nb–Ni, Nb–Zr, and Nb–Nb coordination.

The first nearest neighbor peaks at $r\sim2.2$ Å of the FT spectra for the Zr *K*-edge are assigned to the Zr–Ni coordination [Fig. 2(c)], as described above. The second nearest neighbor peaks at $r\sim3.0$ Å seem to mostly come from the Zr–Zr and Zr–Nb coordination. In addition, there will be the effective component of the Ni–Ni coordination to the peak to some extent.

As can be seen in Fig. 2, there is a close resemblance between the FT spectra of Zr30–H0 and Zr30–H9 for each absorption edge. On the other hand, the FT spectra of Zr40–H0 are clearly different from those of Zr40–H11. The height of first nearest neighbor peak of the Zr40 alloy decreases significantly for all the three *K*-edges after hydrogen charging. There is also a significant difference between Zr40–H0 and Zr40–H9 in the shape of FTs of the Nb and Zr *K*-edges around $r=2.6-3.5$ Å. These results clearly indicate that hydrogen doping essentially does not alter the local structures around the three atoms for the Zr30 alloy but fairly modifies those for the Zr40 alloy.

B. Curve-fitting analysis

In order to obtain the more quantitative structural parameters (N,r,σ^2) around the core-excited atoms, the fine analysis by curve-fitting techniques was carried out.

The curve-fitting results for the Nb *K*-edge are summarized in Table I. Only the first neighbor peaks are treated in the ranges of $R=1.7-2.8$ Å for the Zr40–H11 alloy and $R=1.7-2.5$ Å for other glassy alloys in the curve-fitting analysis. Here we assume that each peak consists of one structural component (one-shell model), i.e., Nb–Ni alone, in the analysis.[28] The interatomic distances obtained are close to the Nb–Ni interatomic distance for the reported atomic structures of NiNb crystal alloys.[22,23] For the Zr30 alloy, there are no differences in the interatomic distance (r), the coordination number (N), and MSRD (σ^2) between alloys with and without hydrogen within the analytical limit. On the other hand, the interatomic distance in the Zr40 alloys becomes longer, and the coordination number and MSRD become larger after hydrogenation. The peak corresponding to the first nearest neighbor shows an asymmetrical form after the hydrogenation [see Fig. 2(a). This suggests that the two structural factors are contained in the first nearest neighbor peak of the Zr40–H11 alloy. Thus, the "one-shell model" seems to be not appropriate for this peak of Zr40–H11 alloy.

The results of the curve-fitting analysis for the Zr *K*-edge are summarized in Table II. The first and second nearest

TABLE I. Results of curve-fitting analysis for Nb *K*-edge. The interatomic distances (r), the coordination numbers (N), $\Delta E_0 = E - E_0$, and the MSRDs (σ^2) for all four glassy alloys obtained by the analysis are shown. The values of *R*-factor are also given at the bottom.

Bond		Zr30–H0	Zr30–H9	Zr40–H0	Zr40–H11
Nb–Ni	r/Å	2.55	2.54	2.54	2.59
	N	1.5	1.5	0.90	1.6
	ΔE_0/eV	−5.3	−7.0	−6.3	−3.7
	σ^2/Å^2	0.0086	0.0088	0.0069	0.013
	R-factor	0.0022	0.0031	0.0093	0.051

neighbor peaks are treated in the fitting analysis ($R = 1.75-3.3$ Å). In the analysis, we assumed that these peaks consist of two components, i.e., "two-shell model." The first nearest neighbor peak more likely consists of Zr–Ni coordination only. The second nearest neighbor peak probably consists of two major components, i.e., Zr–Zr and Zr–Nb. However, we collected the two components into one shell. The functions $F_i(k)$, $\lambda_\iota(k)$, and $\lambda_\iota(k)$ used in this shell are calculated by the Zr–Zr single scattering path. This treatment is valid because Nr and Zr adjoin in the atomic number, resulting in a very small difference in functions $F_i(k)$, $\phi_\iota(k)$, and $\lambda_\iota(k)$ between Zr–Nb and Zr–Zr scattering paths.

As can be seen in Table II, the Zr–Ni bond lengths for the Zr30 and Zr40 alloys are almost identical (2.63–2.64 Å), independent of hydrogen contents. The coordination numbers of the Zr30 alloys are significantly larger than those of the Zr40 alloys, reflecting the difference in Zr concentration between these glassy alloys. The Zr–Zr/Zr–Nb distances between the Zr30–H0 and the Zr30–H9 alloys are the same within experimental accuracy. On the other hand, the Zr–Zr/Zr–Nb distance of the Zr40–H11 alloy is fairly longer than that of the Zr40–H0 alloy by 0.08 Å. The hydrogen-induced expansion of the Zr–Zr distance has been also reported by Sakurai *et al.*[15] on $(Ni_{0.6}Nb_{0.4})_{100-x}Zr_x$ ($x=30$, 50) glassy alloys by the Zr *K*-edge XAFS and x-ray diffraction[16] and by Liu *et al.*[29] on $NiZr_2$ by the Zr *K*-edge XAFS. Furthermore, the Nb–Ni distance of the Zr40–H11 alloy also expands compared with that of the Zr40–H0 one, although there is no report concerning the expansion.

The difference in the structural response between Zr30 and Zr40 alloys probably comes from the difference in site where hydrogen atoms are located, as we will explain in detail later in Sec. IV. In Zr30 alloy, hydrogen atoms plunge into somewhere outside the clusters, since no significant change in bond length was observed. The elongation of Zr–Zr/Zr–Nb and Nb–Ni distances in Zr40–H11 alloy is associated with an occupation of hydrogen in tetrahedral sites surrounded by Zr and Nb or Zr, Nb, and Ni atoms in the clusters.

For the Ni *K*-edge, the first nearest neighbor peak is probably derived from at least three contributions (Ni–Ni, Ni–Nb, and Ni–Zr), as discussed above. Consequently, the number of the fitting parameters becomes so large that we could not obtain reliable fitting results, even if the interatomic distances and MSRDs of Ni–Nb and Ni–Zr are constrained to those obtained in the fitting analysis of the Nb and Zr *K*-edges. To enhance the performance of the curve-fitting analysis on the data of the Ni *K*-edges, we must increase the restriction condition for the fitting parameters. This will provide to construct concrete atomic cluster models.

IV. DISCUSSION

It is known that icosahedronlike polyhedra play an important role to stabilize the structure of metal-metal-type glassy alloys.[13] With this fact in mind, we will discuss the possible structural models for the Ni–Nb–Zr glassy alloy studied here.

First, we examine the model reported by Fukunaga *et al.*[13] Their results on the analysis of Voronoi polyhedra in the reverse Monte Carlo simulation based on the data of neutron and x-ray diffraction indicate that *all* the Zr atoms in the $Ni_{25}Zr_{60}Al_{15}$ metallic glass are mostly surrounded by icosahedra or icosahedronlike polyhedra. This means that the average coordination number for Zr atom is ~12. However, the coordination numbers estimated from our XAFS results are

TABLE II. Results of curve-fitting analysis for Zr *K*-edge. For details, see the caption for Table I.

Bond		Zr30–H0	Zr30–H9	Zr40–H0	Zr40–H11
Zr–Ni	r/Å	2.63	2.64	2.63	2.64
	N	3.3	3.6	2.6	2.2
	ΔE_0/eV	−7.0	−6.3	−7.5	−10.3
	σ^2/Å^2	0.011	0.012	0.011	0.013
Zr–Zr or Zr–Nb	r/Å	3.24	3.25	3.25	3.33
	N	5.4	4.8	5.1	5.0[a]
	ΔE_0/eV	2.3	2.9	1.8	−0.1
	σ^2/Å^2	0.025	0.025	0.022	0.024
	R-factor	0.0039	0.0044	0.010	0.017

[a]The coordination number of Zr–Zr (Zr–Nb) bond is kept fixed to $N=5.0$ and other parameters r, ΔE_0, and σ^2 were adjusted during the fitting analysis for Zr40–H11.

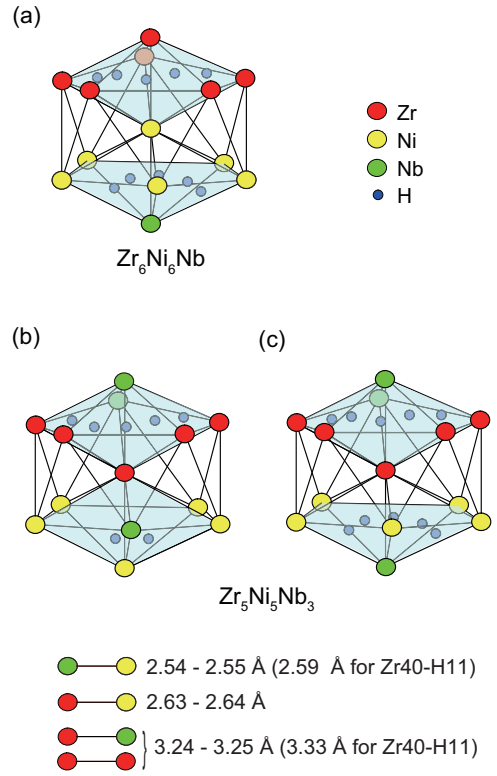

FIG. 3. (Color) Cluster models having the icosahedral structure with the chemical compositions of (a) Zr_6Ni_6Nb and [(b) and (c)] $Zr_5Ni_5Nb_3$. The sites which can be occupied by hydrogen atoms are also indicated by small blue circles. The bond lengths obtained by the XAFS analysis are indicated in the bottom part.

7.2–8.7. Thus the Fukunaga's model is inconsistent with our results of the XAFS analysis.

Then, we will discuss a model in which the icosahedral or icosahedronlike clusters are rather randomly packed. In this model, the contribution from the atoms in neighboring clusters to the FT spectra of XAFS will be negligibly small because it is evident that the positional correlation between the atoms in one cluster and in another one is weak in amorphous state. The configuration of the atoms within a cluster can be much accounted for the coordination numbers observed by XAFS. In the analysis of the Zr *K*-edge XAFS spectra of the Ni–Nb–Zr glassy alloys, Sakurai *et al.*[15] presumed that the second nearest neighbor peak in FT spectra mostly comes from the Zr–Zr bonds, and the contribution from Zr–Nb is negligible. This means that the Zr and Nb atoms are not bonded directly. The icosahedral cluster model satisfying this condition [hereafter referred to as model (a)] is depicted in Fig. 3(a). The average coordination numbers calculated for the model (a) are listed in Table III together with the coordination numbers estimated by XAFS analysis for the Zr30–H0 and Zr40–H0 alloys. As given in Table III, the average coordination number of 6 for Nb–Ni estimated from the model (a) is apparently large in comparison with the values obtained by XAFS analysis. Furthermore, the content ratio of Nb to the other atoms (Zr and Ni) in the cluster is too small, taking the actual chemical compositions of the Zr30 and Zr40 alloys into consideration. Thus, it is more likely that the second neighbor peak of the Zr *K*-edge also includes the inevitable component of Zr–Nb as well as that of Zr–Zr.

As the previous models described above would hardly explain the analysis results of the XAFS spectra, we propose two probable cluster models for the Zr–Nb–Ni ternary glassy alloys, as depicted in Figs. 3(b) and 3(c) [hereafter referred to as models (b) and (c), respectively]. In fact, the average coordination numbers calculated for both cluster models (Table III) fairly agree with the coordination numbers estimated by XAFS. It should be noted that the shape of the icosahedron should be distorted since the bond lengths of Zr–Ni, Nb–Ni, Zr–Zr, and Zr–Nb are different among them, as shown in Fig. 3.

In both models, the maximum numbers of hydrogen atoms which can be stored in the clusters are different. From XAFS analysis, it is difficult to determine which model is more preferable since the difference between the coordination numbers calculated for models (b) and (c) is so small in the accuracy of coordination number obtained by XAFS analysis. The distorted icosahedral cluster(s) of models (b) and (c) or the combination of models (b) and (c) will be the main constituent(s) of glassy alloys.

The addition of hydrogen atoms has no significant effect on the atomic configuration in Zr30 alloy but on the Zr40 one. This suggests that hydrogen atoms not only occupy the sites outside the Ni–Nb–Zr clusters in Zr30 alloys but both inside and outside the clusters in Zr40 alloys. This difference in the location of hydrogen atoms possibly comes from a certain structural difference between Zr30 and Zr40 alloys. Although we have not had a clear picture yet, there may be a structural difference in the cluster itself and/or that in the interstitial space outside the cluster defined by the manner in which clusters are arranged in the alloys.

From the structural change in the hydrogenated Zr40 alloy observed by XAFS analysis, we can decide the occupation sites of hydrogen, as indicated by small blue solid circles in Fig. 3. In the upper part of the clusters, hydrogen atoms are settled into the tetrahedron sites that are surrounded by three Zr atoms and one Nb atom, since the Zr–Zr

TABLE III. Average coordination numbers calculated for three cluster models. The structures of model clusters are illustrated in Fig. 3. The coordination numbers estimated by XAFS analysis are also shown.

		Model			XAFS	
Edge	Bond	(a)	(b)	(c)	Zr30–H0	Zr40–H0
Nb *K*	Nb–Ni	6	1.67	2.33	1.5	0.90
	Nb–Nb or Nb–Zr	0	4.33	3.67	···	···
Zr *K*	Zr–Ni	2.6	2.2	2.6	3.3	2.6
	Zr–Zr or Zr–Nb	3.4	5	4.6	5.4	5.1

and Zr–Nb bonds expand after hydrogenation. The Nb–Ni bond also lengthens by hydrogenation. Thus, the hydrogen atoms are plunged into near Nb atom in tetrahedral sites in the lower part of the clusters. More hydrogen atoms favor to occupy in the upper side. Considering the stoichiometry, these sites will be partially occupied by hydrogen atoms in Zr40–H11 alloy.

The atomic radii of Ni, Nb, and Zr in the crystalline form are 1.24, 1.45, and 1.60 Å, respectively.[30] Thus, the atomic distances of Nb–Ni and Zr–Ni in the Ni–Nb–Zr glassy alloys obtained in the present study (2.54–2.55 and 2.63 Å, respectively) are considerably shorter than those calculated from the crystalline atomic radii (2.69 and 2.84 Å, respectively). This is an important point for application of glassy alloys such as superconductivity and ballistic transport. Furthermore, doping of hydrogen atom into the designated tetrahedral sites induces shrinkage of the atomic distances at the neighbor sites as high pressure effect. This also provides another important effect for atomic structural elucidation of various electronic transport behaviors[31] in the Ni–Nb–Zr glassy alloys of interest.

V. CONCLUSION

The local structures around the Ni, Nb, and Zr atoms of the Ni–Nb–Zr glassy alloys and their hydrogenated ones are investigated through the XAFS technique. Hydrogenation does not alter the local structures around the three atoms for the Zr30 alloy but lengthens the interatomic distances of Zr–Zr, Zr–Nb, and Nb–Ni for the Zr40 alloy. Two kinds of the distorted icosahedral $Zr_5Ni_5Nb_3$ clusters are proposed for the possible structural models for Ni–Nb–Zr glassy alloys. If they are assembled in randomly packed manner, the coordination numbers obtained by XAFS analysis are well explained. The elongation observed in the Zr40 alloy implies that the hydrogen atoms are plunged into the tetrahedral Zr–Nb sites and the sites near the Nb atom surrounded by (Nb and Ni) or (Nb, Ni, and Zr) atoms. On the other hand, hydrogen atoms seem to occupy the interstitial site between clusters in the Zr30 alloy. Considering the crystalline atomic radii of Ni, Nb, and Zr atoms, the atomic distances of Nb–Ni and Zr–Ni in the alloys are considerably short.

ACKNOWLEDGMENTS

This work was supported by a Grant-In-Aid for Science Research in a Priority Area "Research and Development Project on Advanced Metallic Glasses, Inorganic Materials and Joining Technology" from the Ministry of Education, Science, Sports and Culture of Japan and by JSPS Asian CORE Program. The synchrotron radiation experiments were performed with the approval of the Japan Synchrotron Radiation Research Institute (JASRI) (Proposal No. 2007B1820). One of the authors (H.O.) wishes to thank Dr. I. Hirosawa of Japan Synchrotron Radiation Research Institute for the careful reading of the manuscript and helpful advice.

[1] E. Ben-Jacob and Y. Gefen, Phys. Lett. **108A**, 289 (1985).
[2] M. A. Kastner, P. F. Kwasnick, and J. C. Licini, Phys. Rev. B **36**, 8015 (1987).
[3] T. A. Fulton and G. J. Dolan, Phys. Rev. Lett. **59**, 109 (1987).
[4] M. Stopa, Phys. Rev. Lett. **88**, 146802 (2002).
[5] K. M. Birnbaum, A. Boca, R. Miller, A. D. Boozer, T. E. Northum, and H. J. Kimble, Nature (London) **436**, 87 (2005).
[6] M. Fukuhara, A. Kawashima, S. Yamaura, and A. Inoue, Appl. Phys. Lett. **90**, 203111 (2007).
[7] M. Fukuhara and A. Inoue, Europhys. Lett. **83**, 36002 (2008).
[8] M. Fukuhara, S. Yamamura, and A. Inoue, Phys. Status Solidi B **246**, 153 (2009).
[9] M. Fukuhara and A. Inoue, J. Appl. Phys. **105**, 063715 (2009).
[10] D. G. Westlake, H. Shaked, P. R. Mason, B. R. McCart, M. H. Mueller, T. Matsumoto, and M. Amano, J. Less-Common Met. **88**, 17 (1982).
[11] K. Suzuki, N. Hayashi, Y. Tomizuka, T. Fukunaga, K. Kai, and N. Watanabe, J. Non-Cryst. Solids **61–62**, 637 (1984).
[12] E. Matsubara, T. Tamura, Y. Waseda, A. Inoue, T. Zhang, and T. Masumoto, Mater. Trans., JIM **33**, 873 (1992).
[13] T. Fukunaga, K. Itoh, T. Otomo, K. Mori, M. Sugiyama, H. Kato, M. Hasegawa, A. Hirata, Y. Hirotsu, and A. C. Hannon, Mater. Trans. **48**, 1698 (2007).
[14] T. Takeuchi, S. Nakano, M. Hasegawa, K. Soda, H. Sato, U. Mizutani, K. Ito, and T. Fukunaga, Mater. Trans. **46**, 2791 (2005).
[15] M. Sakurai, S. Yamaura, K. Wakoh, E. Matsubara, and A. Inoue, J. Metastable Nanocryst. Mater. **24–25**, 551 (2005).
[16] S. Yamaura, M. Sakurai, M. Hasegawa, K. Wakoh, Y. Shimpo, M. Nishida, H. Kimura, E. Matsubara, and A. Inoue, Acta Mater. **53**, 3703 (2005).
[17] H. Kimura, A. Inoue, S. Yamaura, K. Sasamori, M. Nishida, Y. Shinpo, and H. Okouchi, Mater. Trans. **44**, 1167 (2003).
[18] S. Yamaura, Y. Shimpo, H. Okouchi, M. Nishida, O. Kajita, H. Kimura, and A. Inoue, Mater. Trans. **44**, 1885 (2003).
[19] *X-ray Absorption Principles, Applications, Techniques of EXAFS, SEXAFS, and XANES*, edited by D. C. Koningsberger and R. Prins (Wiley, New York, 1988).
[20] http://www.spring8.or.jp/wkg/BL14B2/instrument/lang-en/INS0000001470/instrument_summary_view.
[21] B. Ravel and M. Newville, J. Synchrotron Radiat. **12**, 537 (2005).
[22] A. Kaufman, N. J. Hoffman, and H. Lipson, Scr. Metall. **3**, 715 (1969).
[23] T. Fang, S. J. Kennedy, L. Quan, and T. J. Hicks, J. Phys.: Condens. Matter **4**, 2405 (1992).
[24] M. Bououdina, B. Lambert-Andron, B. Ouladdiaf, S. Pairis, and D. Fruchart, J. Alloys Compd. **356-357**, 54 (2003).
[25] E. E. Havinga, H. Damsma, and P. Hokkeling, J. Less-Common Met. **27**, 169 (1972).
[26] J. M. Da C. Brochado Oliveira and I. R. Harris, J. Mater. Sci. **18**, 3649 (1983).
[27] C. Becle, B. Bourniquel, G. Develey, and M. Saillard, J. Less-Common Met. **66**, 59 (1979).
[28] Because of the relatively complicated shapes of FTs in the second nearest neighbor region (at least there seems to be two structural components), a multishell model with more than two shells would be needed for the curve-fitting analysis including the first and second nearest neighbor peaks. However it is hardly possible to analyze the Nb *K*-edge data by the multishell model since the FT amplitude in the second neighbor region is weak and the structure is not well resolved.
[29] X. J. Liu, X. D. Hui, H. Y. Hou, T. Liu, and G. L. Chen, Phys. Lett. A **372**, 3313 (2008).
[30] *International Tables for X-ray Crystallography* (Kynoch, Birmingham, 1968), Vol. III, p. 166.
[31] M. Fukuhara, H. Yoshida, K. Koyama, A. Inoue, and Y. Miura, Europhys. Lett. (submitted).